J. Fluid Mech. (1986), *vol.* 171, *pp.* 183–207
Printed in Great Britain

Film-splitting flows in forward roll coating

By D. J. COYLE†, C. W. MACOSKO AND L. E. SCRIVEN

Department of Chemical Engineering and Materials Science, University of Minnesota, Minneapolis, MN 55455, USA

(Received 6 May 1985 and in revised form 1 April 1986)

A model based on the lubrication approximation is put forward for the general case of asymmetric forward roll coating of Newtonian liquids. Two more-rigorous theories are developed, one based on asymptotic expansions for small ratios of gap-to-roll diameter (H_0/R), the second on Galerkin/finite-element solutions of the full Navier–Stokes equations over the relevant flow domain. The lubrication model is useful only as an approximation at high capillary numbers ($Ca \equiv \mu\bar{V}/\sigma$). The asymptotic analysis is accurate when $H_0/R < 0.001$ and $Ca > 0.1$. The ratio of the film thicknesses on the two rolls is predicted to equal the speed ratio to the 0.65 power, which is confirmed experimentally. The Galerkin/finite-element solutions give full details of the steady two-dimensional free-surface flows including complex recirculation patterns in the film-splitting region, and show how the film-splitting stagnation line becomes a static contact line in the limit as one roll surface becomes stationary.

1. Introduction

Forward roll coating is a process whereby liquid flows into a narrow gap between two rotating cylinders (or a rotating cylinder and a translating flat sheet), the non-deformable surfaces of which move in the same direction. Some of the liquid passes through the gap and a short distance downstream splits into two films, each coating one of the rolls. The flow may be symmetric, as shown in figure 1, or it may be made asymmetric by unequal roll radii or speeds. The rolls need not be half-submerged, as shown in figure 1; indeed, it is common for just one of the rolls to bring a liquid film into the gap and the other to arrive dry. There are other situations such as in multi-roll printing presses where film-splitting is used to meter and distribute liquid, and both rolls may bring liquid films to the gap.

This paper analyses these flows from three perspectives: (i) classical lubrication theory (see Cameron 1966; Middleman 1977), (ii) asymptotic expansions such as those derived by Ruschak (1982), and (iii) solution of the Navier–Stokes system in the relevant flow domain by the Galerkin/finite-element method. The lubrication model is developed in full generality, so that configurations with equal roll radii, equal surface speeds, or one surface stationary arise naturally as special cases. In a similar fashion Ruschak's asymptotic equations are generalized to the asymmetric case and solved. Finally the viscous free-surface flows are calculated in detail by solving the Navier–Stokes system. The results not only provide a test of the validity of the simple model and the asymptotic approximation but also set the stage for accurate three-dimensional linear stability analysis presented elsewhere (Coyle 1984; Coyle, Macosko & Scriven 1986*a*).

† Present address: General Electric Company, Corporate Research and Development, Schenectady, NY 12301, USA.

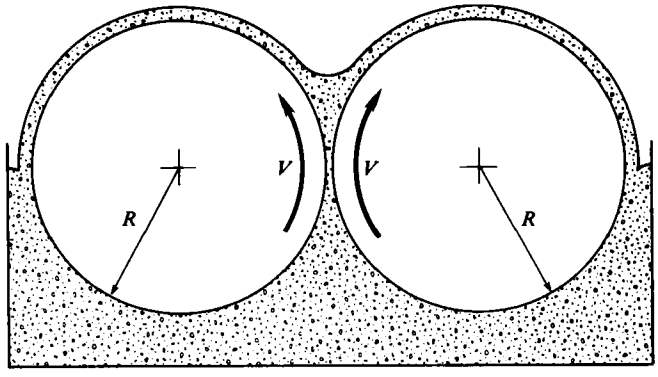

FIGURE 1. Symmetric film splitting in a half-submerged forward roll coating flow.

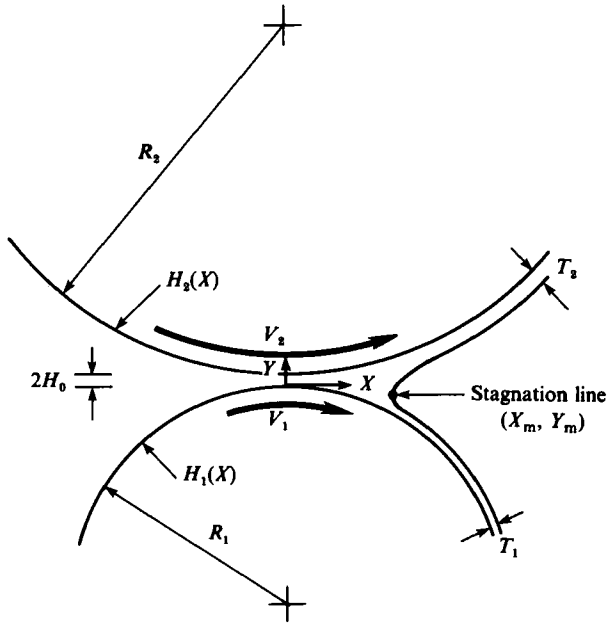

FIGURE 2. Definition sketch of asymmetric film splitting in forward roll coating with half-submerged rolls.

2. Lubrication theory for a Newtonian liquid

In setting up a lubrication model of these flows it is convenient to define the dimensionless coordinates

$$\xi \equiv \frac{X}{(RH_0)^{\frac{1}{2}}}, \quad y \equiv \frac{Y}{H_0}, \tag{2.1}$$

where H_0 is the half-gap width and R is the average roll radius (see figure 2)

$$\frac{1}{R} \equiv \frac{1}{2}\left(\frac{1}{R_1}+\frac{1}{R_2}\right).$$

A transformed X-coordinate θ and a transformed Y-coordinate η are defined by

$$\theta \equiv \tan^{-1}\left(\frac{\xi}{\sqrt{2}}\right), \quad \eta \equiv 2\frac{Y-H_1(X)}{H_2(X)-H_1(X)}, \tag{2.2}$$

so that $-\frac{1}{2}\pi \leqslant \theta \leqslant \frac{1}{2}\pi$ and $0 \leqslant \eta \leqslant 2$, where the roll surface profiles though circular are approximated by parabolas

$$H_1(X) \equiv -\frac{X^2}{2R_1}, \quad H_2(X) \equiv 2H_0 + \frac{X^2}{2R_2}.$$

In terms of these variables the dimensionless separation between roll surfaces is simply given by

$$\frac{H_2(X)-H_1(X)}{H_0} = \xi^2 + 2 = \frac{2}{\cos^2\theta}. \tag{2.3}$$

The speed ratio and average roll speed are defined as

$$V \equiv \frac{V_2}{V_1}, \quad \overline{V} \equiv \tfrac{1}{2}(V_1 + V_2),$$

and the dimensionless variables defined by

$$p \equiv \frac{PH_0}{\mu\overline{V}}\left(\frac{H_0}{R}\right)^{\frac{1}{2}}, \tag{2.4}$$

$$u \equiv \frac{U}{\overline{V}}, \tag{2.5}$$

$$\lambda \equiv \frac{\frac{1}{2}\int_{H_1}^{H_2} U\,\mathrm{d}Y}{\overline{V}H_0}, \tag{2.6}$$

are the pressure, x-velocity, and flow rate through the gap. In the limit of the lubrication approximation the balance of X-momentum reduces to

$$u_{\eta\eta} = \tfrac{1}{4}(\xi^2+2)^2 p_\xi. \tag{2.7}$$

No-slip boundary conditions at the roll surfaces are

$$u(\eta = 0) = \frac{2}{1+V}, \quad u(\eta = 2) = \frac{2V}{1+V}, \tag{2.8}$$

so that integrating (2.7) twice with respect to η gives

$$u = \frac{(\xi^2+2)^2}{8}p_\xi(\eta^2-2\eta) + \frac{V-1}{V+1}\eta + \frac{2}{V+1}. \tag{2.9}$$

Substituting this result in (2.6) and rearranging gives

$$p_\xi = \frac{12}{(\xi^2+2)^2} - \frac{24\lambda}{(\xi^2+2)^3}. \tag{2.10}$$

In terms of θ, the transformed x-coordinate, the velocity field and pressure gradient field are

$$u = \tfrac{3}{2}(1-\lambda\cos^2\theta)(\eta^2-2\eta) + \frac{V-1}{V+1}\eta + \frac{2}{V+1}, \tag{2.11}$$

$$p_\theta = p_\xi \xi_\theta = 3\sqrt{2}(\cos^2\theta - \lambda\cos^4\theta). \tag{2.12}$$

Integrating the latter for half-submerged rolls, i.e. with $p(-\frac{1}{2}\pi) = 0$, gives the pressure profile

$$p/3\sqrt{2} = -\tfrac{1}{4}\lambda \sin\theta \cos^3\theta + (1-\tfrac{3}{4}\lambda)(\tfrac{1}{2}\theta + \tfrac{1}{4}\sin 2\theta + \tfrac{1}{4}\pi). \tag{2.13}$$

The dimensionless flow rate λ is determined by specifying another boundary condition on pressure.

The simplest case is that of completely submerged rolls (cf. Gatcombe 1945; Banks & Mill 1954), for which $p(\frac{1}{2}\pi) = 0$; this leads to the result

$$\lambda = \tfrac{4}{3}. \tag{2.14}$$

Another possible boundary condition is that of Reynolds' (1886), a postulate that at some point in the flow (here denoted with the subscript m) both the pressure and its gradient vanish. Setting to zero the right-hand sides of (2.12) and (2.13) leads to

$$\left.\begin{aligned} \lambda &= 1.226, \\ \theta_{\mathrm{m}} &= 0.4436 \quad (\xi_{\mathrm{m}} = 0.6719). \end{aligned}\right\} \tag{2.15}$$

As discussed by Taylor (1963) and Dowson & Taylor (1979), this boundary condition is most appropriate when the film is split by cavitation within the liquid. Taylor's photographs show a transition from smooth flow separation at the downstream meniscus to irregular, cavitation-induced film splitting, i.e. formation of bubbles of air and/or water vapour within the liquid. Similar evidence of cavitation is presented in the works of Cole & Hughes (1956), of Floberg (1961*a*, *b*, 1964), and of Myers and coworkers (see Miller & Myers 1958; Myers, Miller & Zettlemoyer 1959; Myers & Hoffman 1961; Hoffman & Myers 1962). The analyses presented in the remainder of this paper deal only with the smooth flow-separation regime of film splitting.

A problem with the Reynolds model is that it gives no clue as to how much of the liquid is carried by each roll in the asymmetric case. Savage (1982) resorted to intuitive arguments to arrive at a relationship between the ratio of film thicknesses and the speed ratio, which can be written as

$$\frac{T_2}{T_1} = \frac{V(V+3)}{3V+1}. \tag{2.16}$$

When the film splits by flow separation rather than cavitation, the lubrication approximation requires some sort of model for the flow separation region. Hopkins (1957) postulated that the film splits at the first stagnation point (actually a line perpendicular to the (X, Y)-plane) downstream of the gap centre at a point midway between roll surfaces. This idea can be extended to the asymmetric case as follows. The coordinates of the split point are $(\theta_{\mathrm{m}}, \eta_{\mathrm{m}})$, and at this point

$$p(\theta_{\mathrm{m}}) = -\frac{1}{Ca_1 r_{\mathrm{m}}}, \tag{2.17}$$

$$u(\theta_{\mathrm{m}}, \eta_{\mathrm{m}}) = 0, \tag{2.18}$$

$$\frac{\partial u}{\partial \eta}(\theta_{\mathrm{m}}, \eta_{\mathrm{m}}) = 0, \tag{2.19}$$

where r_{m} is the radius of curvature of the meniscus in units of half-gap width, $Ca_1 \equiv (\mu \overline{V}/\sigma)(R/H_0)^{\frac{1}{2}}$ is a modified capillary number, p is given by (2.13) and u by (2.11). It should be noted that (2.19) is the boundary condition missed by Benkreira, Edwards & Wilkinson (1981*a*) and thus their analysis is incorrect. The three

equations (2.17)–(2.19) are independent and contain four unknowns (λ, θ_m, η_m, r_m): an additional relation is needed. If the meniscus is modelled as an arc of circle between parallel plates (cf. Greener & Middleman 1979), geometry demands that

$$\frac{H_2(X_m)-H_1(X_m)}{H_0}=\frac{2}{\cos^2\theta_m}=2r_m+t_1+t_2, \tag{2.20}$$

where t_1 and t_2 are the final thicknesses, in units of half-gap width, of the films carried by rolls 1 and 2 respectively (i.e. $t_1 \equiv T_1/H_0$, $t_2 \equiv T_2/H_0$). These are two added unknowns, but they are governed by two mass balances. An overall mass balance gives

$$\lambda(V+1)=t_1+t_2 V, \tag{2.21}$$

and a balance around the film on roll 1 gives

$$t_1=\frac{(1+V)}{2\cos^2\theta_m}\int_0^{\eta_m} u(\theta_m,\eta)\,d\eta. \tag{2.22}$$

Now there are six unknowns and six equations: (2.17)–(2.22). The set can be solved numerically as was done by Savage (1982) with an analogous set of equations. This is not the best manner in which to proceed, because some simple analytical results can be derived as follows. The momentum balance (2.7) requires a velocity profile that is quadratic in η:

$$u=a\eta^2+b\eta+c. \tag{2.23}$$

The definition of η (2.2) is such that $0 \leqslant \eta \leqslant 2$, and so at the film-split location (θ_m, η_m) the no-slip (2.8) and stagnation-point conditions (2.18, 2.19) give four equations in the four constants a, b, c, and η_m. Solving these yields

$$\eta_m=\frac{2}{1+V^{\frac{1}{2}}}. \tag{2.24}$$

From this a mass balance gives the film-thickness ratio

$$\frac{t_2}{t_1}=\frac{\int_{\eta_m}^{2} u\,d\eta}{V\int_0^{\eta_m} u\,d\eta}, \tag{2.25}$$

which simplifies to

$$\frac{t_2}{t_1}=V^{\frac{1}{2}}. \tag{2.26}$$

Thus the film-thickness ratio is simply the square root of the speed ratio. A similar relationship has been derived for a power-law liquid (Coyle, Macosko & Scriven 1986*b*). Equating the η^2 (or η) terms in (2.23) and (2.11) makes it possible to solve for θ_m in terms of λ:

$$\lambda\cos^2\theta_m=\frac{2(1-V^{\frac{1}{2}}+V)}{3(V+1)}. \tag{2.27}$$

Combining this result with (2.21) makes it possible to solve for t_1 in terms of λ:

$$t_1=\frac{\lambda(V+1)}{1+V^{\frac{1}{2}}}. \tag{2.28}$$

This result and (2.26) together with (2.20) give the radius of curvature of the meniscus in terms of λ:

$$r_m=\tfrac{1}{2}\lambda(V+1)\left[\frac{3}{1-V^{\frac{1}{2}}+V}-\frac{1+V^{\frac{1}{2}}}{1+V^{\frac{3}{2}}}\right]. \tag{2.29}$$

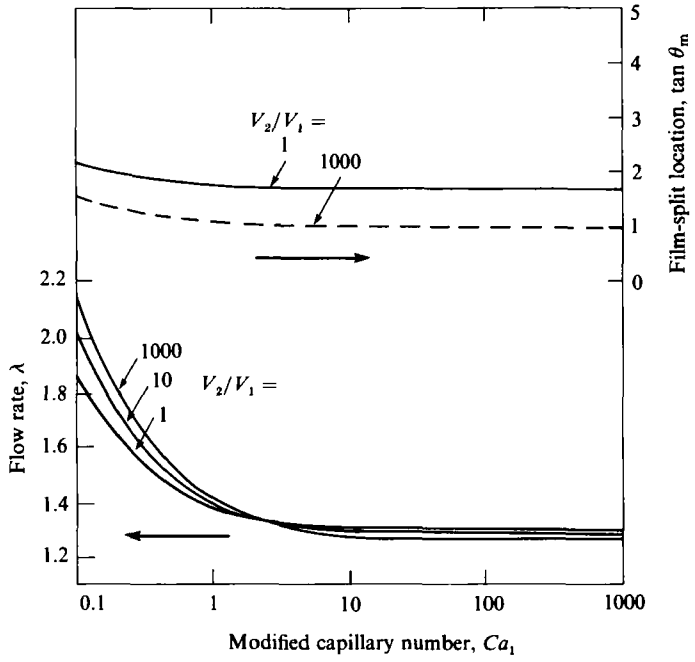

FIGURE 3. Flow rate through the gap (λ) and film-split location ($\tan\theta_m$) predicted by the lubrication-flow model with the hypothesis that the film splits at the first stagnation line.

Thus the pressure boundary condition (2.17) becomes

$$-\tfrac{1}{4}\lambda \sin\theta_m \cos^3\theta_m + (1-\tfrac{3}{4}\lambda)(\tfrac{1}{2}\theta_m + \tfrac{1}{4}\sin 2\theta_m + \tfrac{1}{4}\pi) + \frac{1}{3\sqrt{2}\, Ca_1 r_m} = 0. \quad (2.30)$$

This along with (2.29) and (2.27) gives λ as a function of the parameters Ca_1 and V. When the speed ratio is unity this reduces to the model presented by Greener & Middleman (1979) for that special case. Furthermore, at infinite capillary number the case of unit speed ratio further reduces to the model of Hopkins (1957), according to which

$$\lambda = 1.3015, \quad \tan\theta_m = 1.7044. \quad (2.31)$$

It should be noted that the sheet-and-roll configurations of Taylor (1974) and Greener & Middleman (1975) are also special cases of this general treatment.

At finite capillary number and at speed ratios other than unity, (2.30) is equivalent to the separation model of Savage, who, however, did not report the simple derivation of the film split shown here. Hintermaier & White (1965) attempted this problem but did not find the complete solution; their result for the split ratio is valid only for speed ratios close to unity. As mentioned earlier, Benkreira *et al.* (1981*a*, *b*) missed a boundary condition and in its place used some questionable experimental data to complete the model. In a later paper Benkreira *et al.* (1982) proposed another film-splitting model that rested on an even weaker foundation. How faithful the model presented here is to reality is examined in §4.

Figure 3 shows that the dimensionless flow rate λ is insensitive to capillary number when $Ca_1 > 1$, and falls only slightly as speed ratio rises ($1.30 \geqslant \lambda \geqslant 1.26$). Because Ca_1 is the capillary number, which is often of the order of unity, multiplied by $(R/H_0)^{\frac{1}{2}}$, which is commonly of the order of 1000, the flow rate is nearly constant over most practical operating conditions. The film-split location, also shown in figure 3,

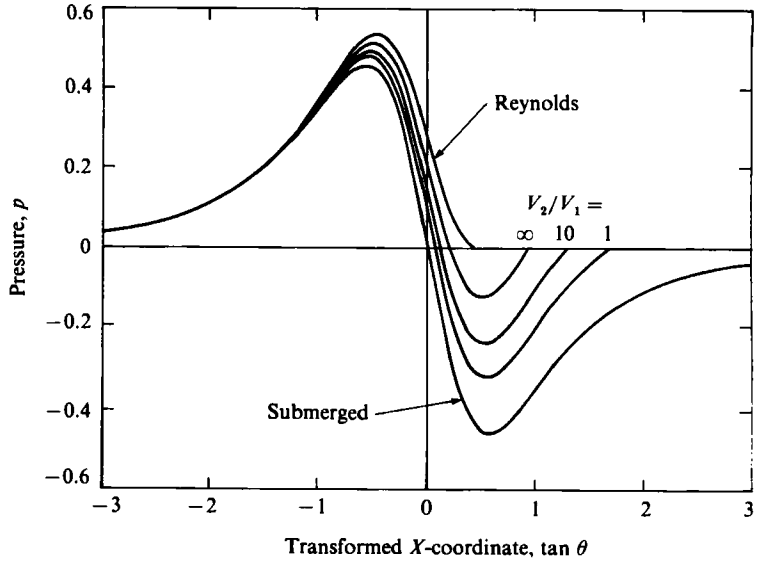

FIGURE 4. Pressure profiles in forward roll coating predicted from lubrication theory ($\tan\theta \equiv X/(2RH_0)^{\frac{1}{2}}$).

is also insensitive to capillary number but recedes somewhat as the speed ratio gets further from unity. Figure 4 shows the characteristic pressure profile that is generated in forward roll coating; it also reveals how maximum pressure climbs and the minimum pressure falls as the speed ratio is increased.

The model presented here should be accurate at high capillary number, but the accuracy is suspect at low capillary number (strong effect of surface tension) because the free-surface model used is crude. This issue is resolved by the analysis in §§4 and 5.

3. Finite-element analysis of steady-state viscous free-surface flows

In all coating flows, not just those of roll coating, there are regions of the flow field that are two-dimensional and bounded by free surfaces, i.e. liquid/air interfaces whose locations are unknown *a priori*. Whereas other regions of the flow may be adequately described by plug-flow or lubrication approximations, these are seldom adequate for the two-dimensional free-surface flows that are crucial to the accurate modelling of coating operations. It is here that the power of the finite-element method is brought to bear.

3.1. *Governing equations and boundary conditions*

For steady, isothermal flow of an incompressible liquid, conservation of momentum and mass is expressed by the Navier–Stokes system, which in dimensionless form is

$$\nabla\cdot\boldsymbol{T} - Re\,\boldsymbol{u}\cdot\nabla\boldsymbol{u} + St\,\boldsymbol{f} = 0, \tag{3.1}$$

$$\nabla\cdot\boldsymbol{u} = 0. \tag{3.2}$$

With a characteristic length L and velocity V, the pressure and stress are made dimensionless by $\mu V/L$, where μ is the liquid viscosity. The total stress $\boldsymbol{T}$ is the sum of the pressure and viscous stress, and for a Newtonian liquid is given by

$\boldsymbol{T} = -p\boldsymbol{I} + [(\nabla \boldsymbol{u}) + \nabla \boldsymbol{u})^{\mathrm{T}}]$. The Reynolds number $Re \equiv \rho VL/\mu$ measures the ratio of inertial to viscous forces and the Stokes number $St \equiv \rho g L^2/\mu V$ measures the ratio of gravity forces to viscous forces. $\boldsymbol{f}$ is a unit vector in the direction in which gravity acts.

Boundary conditions can specify either the velocity or stress. At solid boundaries the no-slip hypothesis is accurate (except very near contact lines), so that Dirichlet or essential boundary conditions are imposed there:

$$\boldsymbol{u} = \boldsymbol{u}_{\mathrm{solid}}. \tag{3.3}$$

Boundary conditions at outflow planes are most often chosen to be Neumann, or natural boundary conditions on the stress, such as the no-traction condition

$$\boldsymbol{n} \cdot \boldsymbol{T} = 0. \tag{3.4}$$

This condition proved adequate for the flows analysed in this work, although a Robin boundary condition that relates the momentum flux to the velocity might have been used to shorten the two-dimensional computational domain (see Bixler 1982). Inflow boundary conditions on the flows of interest here usually arise from a matching of a one-dimensional lubrication-flow model to the two-dimensional flow. The form of this matching is specific to the particular problem at hand; so these boundary conditions are discussed at length where they are used in §§4–6.

At the free surface between the liquid and a gas (considered here as inviscid and inertialess), the normal stress in the liquid must balance the capillary pressure:

$$\boldsymbol{n} \cdot \boldsymbol{T} = \frac{1}{Ca} \frac{\mathrm{d}\boldsymbol{t}}{\mathrm{d}s} - \boldsymbol{n} P_{\mathrm{a}}. \tag{3.5}$$

Here $Ca \equiv \mu V/\sigma$ is the capillary number which characterizes the ratio of viscous to surface tension forces, σ being the surface tension; P_{a} is the ambient gas pressure; $\boldsymbol{t}$ is the unit tangent vector in the direction of increasing arc length s along the free surface; and $\boldsymbol{n}$ is the outward-pointing unit normal vector. Equation (3.5) relates the normal stress in the fluid to surface tension and curvature of the meniscus, and also requires the shear stress to vanish.

At a contact line (which will appear when one of the rolls is stationary) either the location or contact angle must be specified. The downstream end of the free surface is usually taken at an outflow plane, where the appropriate boundary condition for the free surface is that it is parallel to the solid substrate.

In addition to the stress boundary condition at the free surface (3.5), the kinematic boundary condition is also imposed:

$$\boldsymbol{n} \cdot \boldsymbol{u} = 0. \tag{3.6}$$

This requires that there be no mass flow through the interface, i.e. the free surface is a streamline.

3.2. *Finite-element formulation*

The Navier–Stokes system, (3.1) and (3.2) along with associated boundary conditions, is solved by the method of subdomains, finite-element basis functions, and Galerkin's method of weighted residuals. A detailed description of the methodology is given by Kistler & Scriven (1983, 1984) and Kistler (1983). The system is nonlinear owing to the presence of free surfaces, the locations of which are unknown *a priori* and at which nonlinear boundary conditions (3.5) and (3.6) apply. Additional nonlinearity is introduced by the convective momentum transport term in (3.1), but this is seldom significant in roll coating flows, which tend to have small Reynolds numbers.

The first step is to expand the unknown velocity and pressure each in a suitable set of basis functions and subdivide the domain into elements. In the formulation used here, quadrilateral elements are employed, with nine-node biquadratic basis functions (ϕ^i) for the velocity field and four-node bilinear ones (ψ^i) for the pressure field.

The basis-function expansion of the solution is inserted into the governing equations, and the latter are weighted with the basis functions, integrated over the domain, and set to zero. This reduces the original set of partial differential equations (the Navier–Stokes system) to a discrete analogue which takes the form of a large set of nonlinear algebraic equations (vanishing of weighted residuals).

The momentum weighted residual (ϕ^i is the weighting function) provides as many equations as there are velocity unknowns, and the continuity equation (weighted by the pressure basis function ψ^i) provides as many equations as there are pressure unknowns. The kinematic equation is weighted by ϕ^i along the free surface to provide as many equations as there are free-surface parameters.

The coordinates of the nodes under the free surface are functions of the free surface parameters $[h_j]$. When these nodes are located along spines (see Kistler & Scriven 1983), the nodal coordinates $\boldsymbol{x}^k$ of node $k(i,j)$ along the ith spine can be written as

$$\boldsymbol{x}^k = \boldsymbol{x}_{\mathrm{b}}^i + w^j h_i \boldsymbol{e}^i, \tag{3.7}$$

where $\boldsymbol{x}_{\mathrm{b}}^i$ are the coordinates of the base of the spine (usually located on the solid substrate), $\boldsymbol{e}^i$ is a unit vector in the direction along the spine toward the free surface, h_i is the distance along $\boldsymbol{e}^i$ from the base point to the free surface, and w^j are the prescribed proportions according to which the nodes are spaced between the base point and free surface. In addition, the base points $\boldsymbol{x}_{\mathrm{b}}^i$ and the base curve vectors $\boldsymbol{e}^i$ may be functions of other parameters, such as the matching plane XM used in the forward-roll-coating analysis in §§4 and 5.

The key to handling the free surface is the use of isoparametric mapping, an element-by-element transformation between the actual flow domain and replicates of the unit square. Combined with the above node-distribution algorithm, this map allows convenient evaluation of the free-surface location, its unit tangent and normal vectors, and the derivative of any weighted residual equation with respect to the free-surface position.

After the set of algebraic equations is completed with the appropriate boundary conditions, the velocity and pressure fields and the free-surface location can be solved for simultaneously. Essential boundary conditions on the velocities are imposed by replacing the corresponding momentum weighted residual equation at the boundary nodes with the desired velocity specification. Natural boundary conditions are imposed through the boundary integral of $\boldsymbol{n}\cdot\boldsymbol{T}\phi^i$ obtained by integration of the $\nabla\cdot\boldsymbol{T}\phi^i$ term of the momentum equation. For example, no traction at an outflow or symmetry plane is imposed by simply deleting the boundary integral. The stress boundary condition at the free surface is imposed by inserting (3.5) into the boundary integral, integrating by parts, and imposing natural boundary conditions on the slope of the interface at its end points.

3.3. *Evaluation of the basis function coefficients*

As remarked above, the presence of a free surface makes the system of equations governing the flow nonlinear. In most previous attempts to solve such free-surface flows, such as the early work of Nickell, Tanner & Caswell (1974), the free-boundary location has been found by successive approximation techniques. For a given free-surface position, the corresponding flow field is computed with one of the

free-surface boundary conditions omitted, usually the normal-stress condition (the normal component of (3.5)) or the kinematic equation (3.6). That boundary condition, along with the current estimate of the flow field, is used to construct an updated free-surface location, and the cycle is repeated until convergence is obtained. This scheme may or may not converge depending on the choice of the boundary condition used in the iteration and the value of the capillary number (see Silliman 1979; Silliman & Scriven 1980), and even when it is successful the convergence is often slow.

In contrast, Newton's method converges quadratically over the entire parameter range, and has the added bonus that the Jacobian matrix contains information about the stability of the flow, a point which is exploited elsewhere (see Coyle 1984; Coyle *et al.* 1986*a*). Newton iteration was first shown to be superior in solving confined flows by Gartling, Nickell & Tanner (1977). It has only recently been introduced into finite-element analysis of viscous free-surface flows (Ruschak 1980; Saito & Scriven 1981). The biggest difficulty in applying Newton's method is the evaluation of the derivatives of the weighted residuals with respect to the free-surface parameters. But by means of the isoparametric map described in the previous section, the residuals can be written as integrals over the unit (ξ, η) square for each element. Correct differentiation becomes straightforward as described by Kistler & Scriven (1983). Once the Jacobian matrix (the derivatives of the weighted residuals with respect to the finite-element coefficients) is constructed, Newton iteration proceeds to calculate updated coefficients by solving the linear system

$$\boldsymbol{J}\,\Delta\boldsymbol{a} = -\boldsymbol{R}(\boldsymbol{a}_n), \tag{3.8}$$

where $\boldsymbol{a}$ is a vector of finite-element coefficients, and $\Delta\boldsymbol{a} \equiv \boldsymbol{a}_{n+1} - \boldsymbol{a}_n$, the change in coefficients computed during the $(n+1)$th iteration. The iteration proceeds until $\|\Delta\boldsymbol{a}\| < \epsilon$. In practice four norms were required to be less than 10^{-8}: the maximum and the root-mean-square of both the residuals and updates.

In the algorithm used in this work, the full Newton system (3.8) is assembled and solved by the frontal technique developed by Hood (1976, 1977), with the addition of the variable frontwidth modification suggested by Walters (1980).

An initial estimate for Newton iteration is important because the method does not converge if the initial guess is not a close enough approximation to the solution. Zeroth-order continuation was used in this work; i.e. the solution for one set of parameter values is used as an initial estimate for Newton iteration at a not-too-different set of parameters.

The methods of analysis just described were used to compute the steady flows in forward roll coating. In the next section, asymptotic approximations are examined; in §5, full solutions to the Navier–Stokes equations are given.

4. Analysis by the method of matched asymptotic expansions

The biggest difficulty in applying lubrication models to free-surface flows such as those analysed here is supplying appropriate boundary conditions at the liquid/air interface where the liquid splits into two films, one on each roll. As argued by Taylor (1963), the lubrication approximation is valid in the region between the two solid surfaces away from the meniscus, but a local two-dimensional analysis is necessary to describe the flow in the vicinity of the meniscus. Pitts & Greiller (1961) attempted such an analysis of symmetric film-splitting in forward roll coating, but oversimplified the situation near the meniscus. Coyne & Elrod (1970) analysed the free-surface flow between two parallel surfaces, one of which is stationary. Their solution depends on

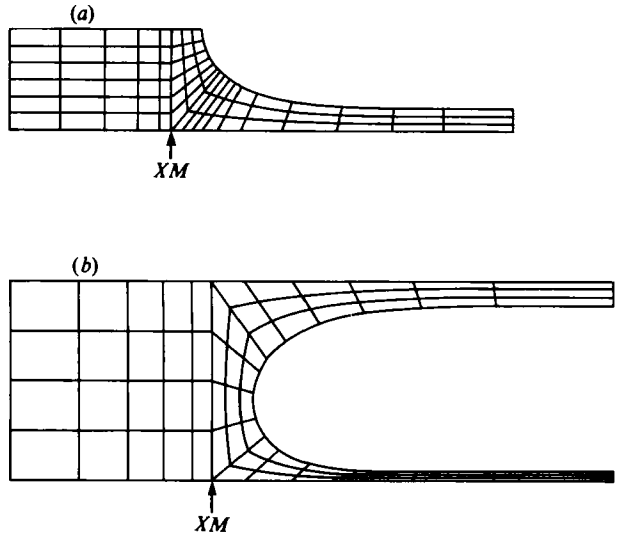

FIGURE 5. Finite-element discretizations for forward roll coating flow in the asymptotic limit of $(H_0/R)^{\frac{1}{2}} \to 0$, i.e. in the limit the roll surfaces become parallel planes ((*a*) symmetric, (*b*) asymmetric).

a number of assumptions, among them that the profile of the velocity component locally parallel to the interface is parabolic in distance from the interface. Nevertheless, it seems generally accepted that their solution provides the most accurate approximate boundary condition available before 1982 for this class of lubrication flows (Savage 1977).

Ruschak (1982) recently showed how these flow problems can be handled with the method of matched asymptotic expansions (see Van Dyke 1975). The lubrication equations arise in the limit as $(H_0/R)^{\frac{1}{2}} \to 0$ when the variables are scaled appropriately for the gap centre as in §2. Equations (2.11) and (2.13) give the x-velocity and pressure, respectively, in the lubrication flow – the outer problem – generalized to the asymmetric case. The variables can also be rescaled for the flow region near the meniscus – the inner problem – the differences being in the x-coordinate and the pressure:

$$x \equiv \frac{X - X_{\mathrm{m}}}{H_0}, \quad p \equiv \frac{PH_0}{\mu \overline{V}}. \tag{4.1}$$

When the variables are scaled in this manner and the limit $(H_0/R)^{\frac{1}{2}} \to 0$ taken, the only simplification of the two-dimensional Navier–Stokes equations is that the domain becomes bounded by parallel plates separated by the distance $H_2(X_{\mathrm{m}}) - H_1(X_{\mathrm{m}})$: see (2.3). In order for the inner and outer flows to be matched, far upstream of the meniscus the inner flow must become rectilinear, i.e.

$$u = \tfrac{3}{2}(1-q)(\eta^2 - 2\eta) + \frac{V-1}{V+1}\eta + \frac{2}{V+1} \quad (x \to -\infty), \tag{4.2}$$

where q is the unknown flow rate measured in units of the average roll speed times one-half the roll separation at the meniscus.

This two-dimensional free-surface flow can be solved by the Galerkin/finite-element method described in §3. Typical discretizations into elements are shown in figure 5 for both the symmetric case and the asymmetric case. The spines whose bases lie on the line XM (the intersection of the matching plane with the (x, y)-plane) pass through

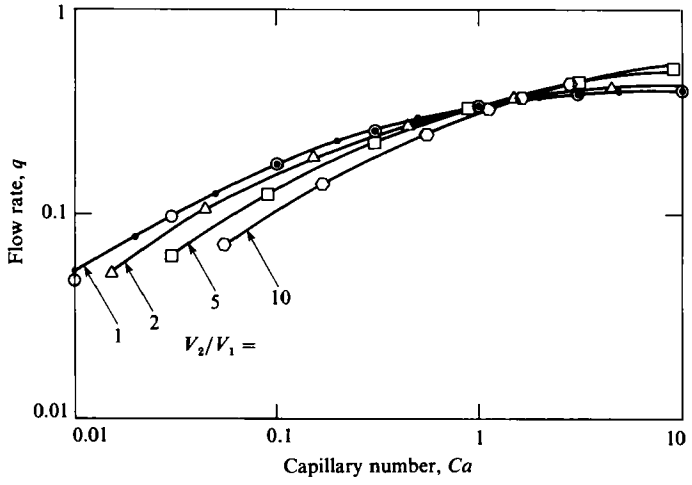

FIGURE 6. Flow rate (q) predicted in the asymptotic limit as $(H_0/R)^{\frac{1}{2}} \to 0$ (open symbols, asymmetric calculation; filled symbols, symmetric calculation).

a polar origin outside the liquid. One of the spines is chosen to locate this origin, and the distance h_j along this spine to the free surface is fixed, as is the distance to the polar origin. Thus the value of this h_j is set as an essential boundary condition. The problem still requires the kinematic equation to be satisfied (the essential boundary condition is imposed by deleting the jth kinematic equation); so the jth kinematic equation is moved to the row of the Jacobian matrix associated with the unknown flow rate q. In this manner the flow rate is determined at the same time as the flow field. In the symmetric case the place where the free surface intersects the symmetry plane is specified to be a stagnation line ($u = v = 0$) and thus the flow field already satisfies the kinematic boundary condition there. But unlike the asymmetric case, a 90° contact angle is required by symmetry and it is this equation which is inserted in the row of the Jacobian associated with q. This equation may be either an essential boundary condition, i.e. the isoparametric map is used to impose directly the slope condition $x_\xi(\xi = 0, \eta = 1) = 0$, or a natural boundary condition, i.e. the x-momentum equation is used to impose the slope in the boundary term which arises from integration by parts of the free-surface boundary integral of the Galerkin weighted residual ($\boldsymbol{i} \cdot \boldsymbol{t}_{\partial\Omega_f} = 0$). The calculated steady flow proves to be insensitive to this choice (to within 3 decimal places).

The distance from the line XM upstream to where the inlet boundary condition (4.2) is imposed is also fixed. This distance must be great enough that the flow field is insensitive to its value (see Ruschak 1982).

Figure 6 shows the flow rate q as a function of capillary number and speed ratio. A much coarser discretization used to calculate the asymmetric film split gave the same q as the finer one used to calculate symmetric split (see figure 5). These results for a speed ratio of unity are the same as those presented by Ruschak (1982) in his figure 3, which also agree well with the approximate solutions of Coyne & Elrod (1970). Changing the speed ratio from unity decreases q when $Ca < 1$ and increases q when $Ca > 1$; it should be noted that the speed in the capillary number is the average roll-surface speed.

The second important variable predicted immediately from the flow calculations near the meniscus is the film thickness ratio t_2/t_1. Figure 7 shows that the split ratio

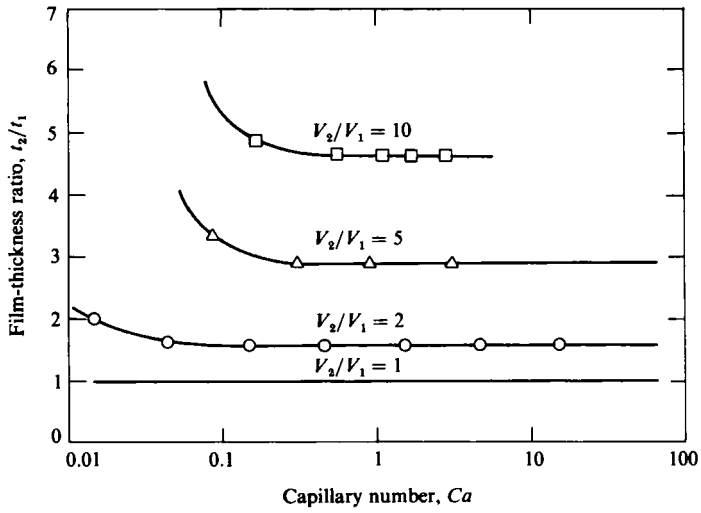

FIGURE 7. Film-thickness ratio predicted in the asymptotic limit as $(H_0/R)^{\frac{1}{2}} \to 0$.

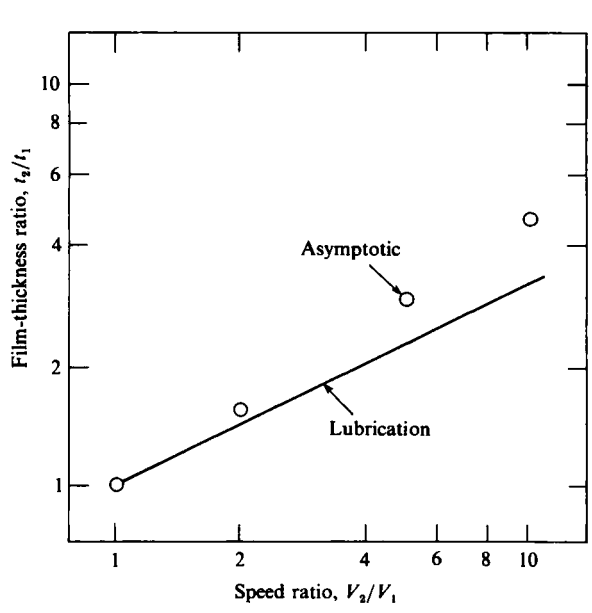

FIGURE 8. Comparison of film-thickness ratios predicted in the asymptotic limit as $(H_0/R)^{\frac{1}{2}} \to 0$, and by lubrication theory with the hypothesis that the film splits at the first stagnation line; both with $Ca \to \infty$.

at a given speed ratio becomes constant at capillary numbers greater than about 0.1. At lower capillary number the effect of disparity in roll radii or surface speeds is exaggerated by capillarity. When the logarithm of film-thickness ratio is plotted versus the logarithm of speed ratio, as in figure 8, the results are close to a line passing through the point (1, 1) with a slope of 0.65. This is higher than the slope of 0.5 predicted by the lubrication model of §2 (2.26), which indicates that the lubrication model is grossly inadequate for describing the asymmetric film splitting.

To complete the solution of the outer problem (the lubrication-flow region) the first

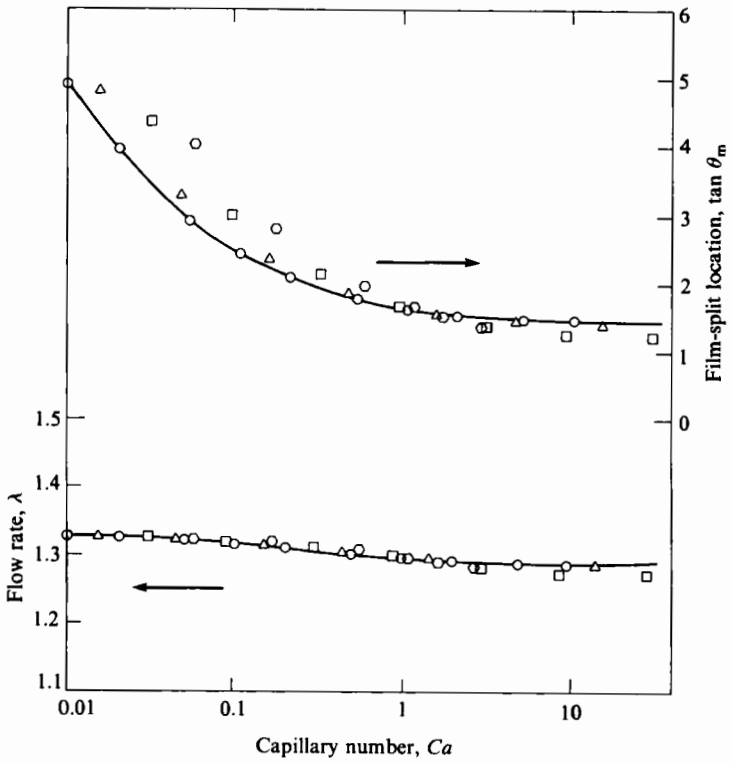

FIGURE 9. Flow rate through the gap (λ) and film-split location ($\tan\theta_m$) predicted in the asymptotic limit as $(H_0/R)^{\frac{1}{2}} \to 0$. —○—, $V = 1$; △, $V = 2$; □, $V = 5$; ⬡, $V = 10$.

terms of the asymptotic expansions are matched to give two boundary conditions (see Ruschak 1982):

$$p(\theta_m) = 0, \tag{4.3}$$

$$p_\theta(\theta_m) = 3\sqrt{2}[\cos^2\theta_m - q\cos^2\theta_m]. \tag{4.4}$$

The pressure and pressure gradient are given by (2.13) and (2.12) respectively; hence the matching conditions become

$$-\tfrac{1}{4}\lambda\sin\theta_m\cos^3\theta_m + (1-\tfrac{3}{4}\lambda)(\tfrac{1}{2}\theta + \tfrac{1}{4}\sin 2\theta + \tfrac{1}{4}\pi) = 0, \tag{4.5}$$

$$q - \lambda\cos^2\theta_m = 0. \tag{4.6}$$

This pair of equations determines the flow rate λ through the gap and the film-split location θ_m as functions of q, which is calculated by solving the inner problem (flow near the meniscus). Figure 9 shows that the flow rate λ is relatively insensitive to both capillary number and speed ratio: at any speed ratio, λ decreases less than 5% as capillary number is increased from 0.01 to infinity. The film-split location, also shown in figure 9, is a strong function of capillary number when $Ca < 1$. Lowering the capillary number causes the meniscus to locate further and further from the gap. The presence of recirculation regions is indicated by a negative minimum x-velocity. Setting $u_\eta = 0$, solving for η, and inserting the result into (4.2) reveals the condition for the presence of recirculation:

$$q \leqslant \frac{2}{3}\left(1 - \frac{V^{\frac{1}{2}}}{V+1}\right). \tag{4.7}$$

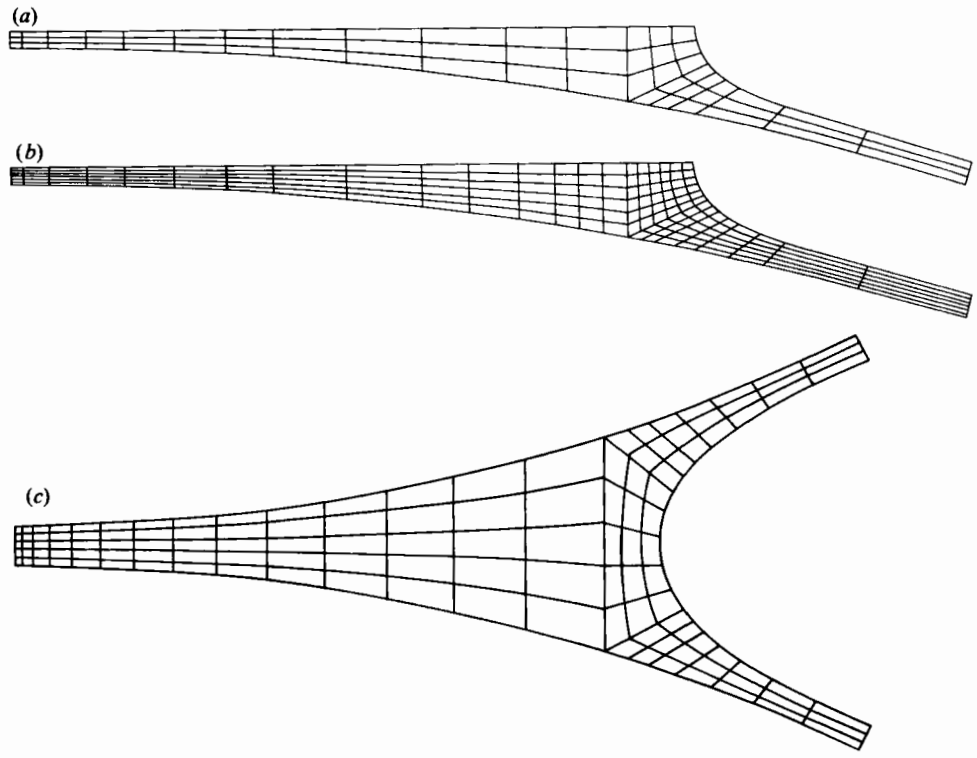

FIGURE 10. Finite-element discretizations for flow in forward roll coating. (*a*) Symmetric, coarse; (*b*) symmetric, fine; (*c*) asymmetric.

By means of figure 6, this roughly translates into the criterion that capillary number be less than unity. Thus as the capillary number falls below unity, recirculations form and the meniscus in turn rises out of the gap to accommodate them. This point is considered further in the next section.

The predictions in this section stand in sharp contrast to those of the lubrication model of §2. The lubrication model predicts that as capillary number is decreased, the film-split location stays relatively constant and the flow rate increases dramatically, while the results of the calculations using the asymptotic expansion predicts the opposite (i.e. flow rate remains constant and film-split location increases dramatically). The reason for this discrepancy will become clear in the following section, which shows the latter prediction to be the correct one.

5. A general analysis of forward roll coating of a Newtonian liquid

The analysis of forward roll coating by the method of matched asymptotic expansions presented in the previous section applies in the limit as $(H_0/R)^{\frac{1}{2}} \to 0$. The question that remains is how accurate the predictions are when roll curvature is appreciable, i.e. when $(H_0/R)^{\frac{1}{2}}$ differs from zero.

The entire flow from the nip to downstream of film splitting was calculated by solving the Navier–Stokes system by the Galerkin/finite-element method outlined above (see also Coyle, Macosko & Scriven 1982). Discretizations for both the symmetric and asymmetric cases are shown in figure 10. The elements are distributed

as in §4, except that the line XM (the base curve for the first few spines used to parametrize the free surface) cannot be specified since the location of the film split is not known *a priori*. XM becomes another variable in the equation set and either the slope boundary condition (symmetric case) or a kinematic equation (asymmetric case) is inserted into the row of the Jacobian matrix associated with the unknown XM, as was done with the variable q in §4.

Boundary conditions are needed at the nip, which constitutes the upstream end of the finite-element domain. Upstream of the nip the flow is known to be well approximated by the equations of the lubrication approximation; accordingly the x-velocity and the pressure are taken from (2.11) and (2.13) respectively. Matching the two flows at $\theta = 0$ (the nip) gives the boundary conditions

$$u = \tfrac{3}{2}(1-\lambda)(\eta^2-2\eta)+\frac{V-1}{V+1}\eta+\frac{2}{V+1}, \tag{5.1}$$

$$v = 0, \tag{5.2}$$

$$p = \tfrac{3}{4}\sqrt{2\pi}\,(1-\tfrac{3}{4}\lambda). \tag{5.3}$$

The velocity profile is specified by replacing the Galerkin weighted residuals of the x- and y-momentum equations at the inlet with (5.1) and (5.2). The flow rate λ is an additional unknown and so (5.3) is inserted into the corresponding row of the Jacobian and this closes the equation set. The pressure used in (5.3) is the average pressure at the inlet plane evaluated with the finite-element basis functions.

Williamson (1972) analysed a related case of creeping flow in similar fashion by using a finite-difference scheme and a sixth-degree polynomial approximation to the free surface. Indeed, Williamson was the first to calculate flow patterns typical of symmetric forward roll coating. He first guessed a value of λ, used a Picard-type iteration (successive approximation) to determine the free surface and flow field, then checked to see if the pressure at the nip was zero. If it was not, he varied the value of λ and repeated the process. This is a highly inefficient scheme because the Picard iteration for the flow field and free surface converges slowly, if at all (see Silliman 1979), and the entire process needs to be repeated at every value of λ. In addition the pressure boundary condition is incorrect, because the pressure at the nip is zero only for totally submerged rolls, in which case $\lambda = \frac{4}{3}$ (see (5.3)). In the present work, Newton iteration was used to solve simultaneously for the flow field, free surface, and flow rate; usually only three or four iterations were needed. In addition, the Jacobian matrix was used to calculate the stability of the flow (see Coyle 1984; Coyle *et al.* 1986*a*).

To test the sensitivity of the calculated flows to the discretization used, the solution obtained with the coarse mesh of 711 unknowns (figure 10*a*) was compared to that obtained with a fine mesh of 1775 unknowns (figure 10*b*). The most sensitive variable, the film-split location, changed by less than 0.1 %, indicating that the coarse mesh gives sufficiently accurate solutions.

Figure 11 shows how the flow field varies with capillary number in the symmetric case. As the capillary number is reduced from 0.5 to 0.3, a pair of eddies forms below the meniscus and moves away from the gap, and the curvature of the meniscus is sharply reduced. It is useful to recognize how to avoid such eddies in which liquid would be trapped forever if the flow were truly steady and two-dimensional, because in reality, which always has some degree of three-dimensionality and unsteadiness, eddies tend to discharge their contents from time to time thus creating certain defects in the coated film.

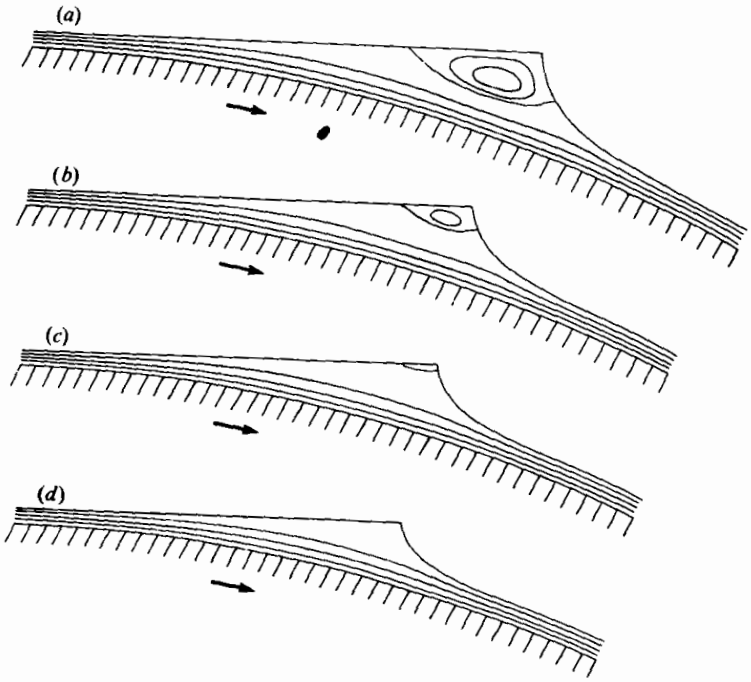

FIGURE 11. Calculated flow fields in symmetric film splitting. $Re = 0$, $St = 0$, $R/H_0 = 100$; (*a*) $Ca = 0.1$; (*b*) $Ca = 0.2$; (*c*) $Ca = 0.3$; (*d*) $Ca = 0.5$.

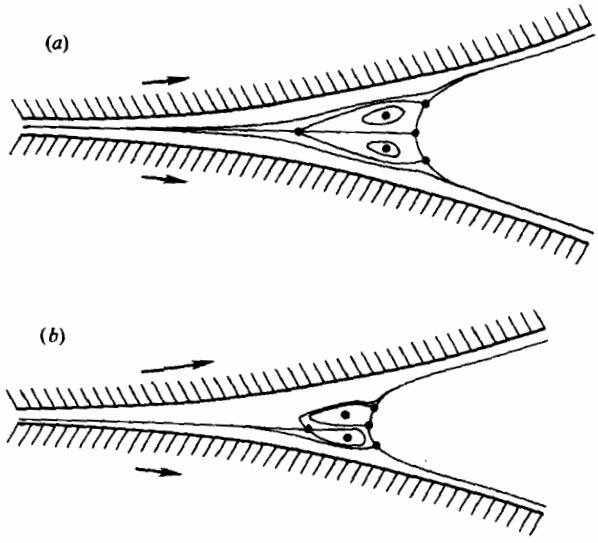

FIGURE 12. Calculated streamlines for symmetric ((*a*) $V = 1$) and asymmetric ((*b*) $V = 2$) flow in forward roll coating. $Ca = 0.1$, $Re = 0$, $St = 0$, $R/H_0 = 200$; ●, stagnation line.

Figure 12 shows how changing the speed ratio breaks the symmetry of the flow. There are still two closed zones of recirculation, but only the one nearer the faster roll is attached to the free surface. The second moves toward the gap slightly, allowing a small amount of liquid to come between it and the slower roll, circulate around its perimeter (between it and the free surface, then between it and the other eddy), and finally form the free surface of the film on the faster roll.

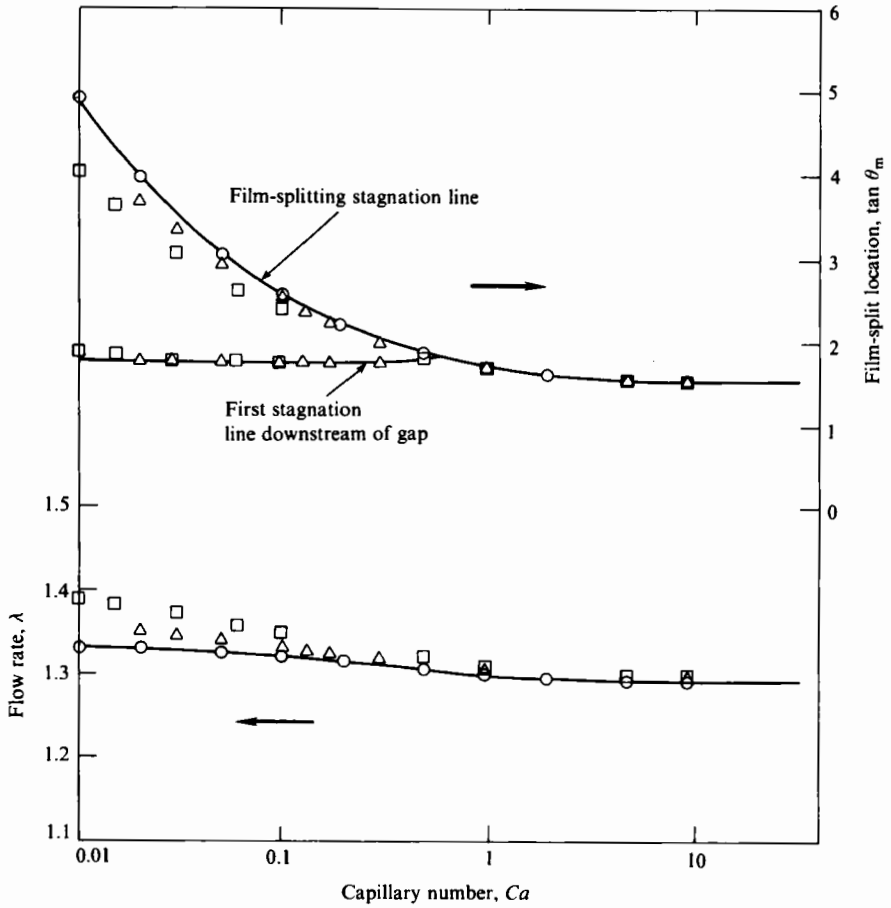

FIGURE 13. Comparison between flow rates (λ) and film-split location ($\tan\theta_m$) for $V = 1$ as predicted by asymptotic analysis and by Navier–Stokes solution. —○—, asymptotic $(H_0/R)^{\frac{1}{2}} \to 0$; △, Navier–Stokes $H_0/R = 0.001$; □, Navier–Stokes $H_0/R = 0.01$.

Figure 13 shows how the flow rate and film-split location converge toward the asymptotic results as H_0/R is decreased. The agreement is good at $H_0/R = 0.001$ for $Ca > 0.1$, while at $H_0/R = 0.01$ the agreement is not good until $Ca > 1$. But even $H_0/R = 0.001$ is a large gap from a practical viewpoint; a typical operating condition might be a 0.001 in. gap with 10 in. diameter rolls, or $H_0/R = 0.0001$. Thus the asymptotic results should be accurate for most applications.

Another important point illustrated in figure 13 is that the location of the first stagnation line downstream of the gap, i.e. the base of the recirculation, is approximately constant with capillary number. As the eddies grow, the meniscus moves further out of the gap to accommodate them. It is this first stagnation line downstream of the gap that is predicted by the lubrication model. In the model this stagnation line is at the free surface, since the model cannot account for the presence of eddies. Boundary condition (2.17) specifies the pressure at this point to be that resulting from the pressure jump across a curved interface, which is completely inappropriate. Thus the lubrication model of §2 incorrectly incorporates surface tension and leads to erroneous predictions of flow rate at low capillary number.

Speed ratio: V_2/V_1	Flow rate λ			Film-split location $\tan\theta_m$		
	Lubrication theory	Asymptotic analysis	GFEM†	Lubrication theory	Asymptotic analysis	GFEM†
1	1.302	1.290	1.293	1.704	1.446	1.458
2	1.299	1.285	1.292	1.639	1.360	1.381
5	1.290	1.271	1.280	1.444	1.145	1.154
10	1.282	—	1.270	1.303	—	0.982
∞	1.255	—	1.233‡	0.939	—	0.7‡

† $H_0/R = 0.001$. ‡ Calculation described in §6.

TABLE 1. Flow rate and film-split location at infinite capillary number as predicted by lubrication theory (stagnation-point boundary condition), asymptotic analysis, and by Galerkin/finite-element solution of the Navier–Stokes equation system over the relevant flow domain

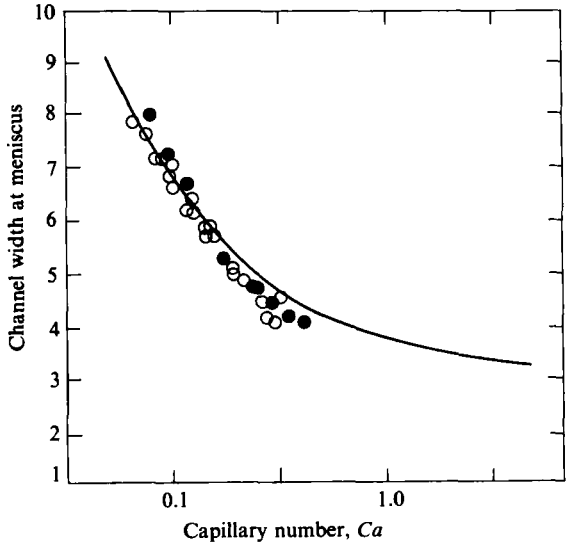

FIGURE 14. Comparison between theoretical prediction and experimental measurements of film-split location. ——, theory; ○, data of Pitts & Greiller (1961); ●, data of this work; channel width $\equiv 1 + X^2/(2RH_0)$.

Table 1 summarizes the predictions of λ and $\tan\theta_m$ at infinite capillary number from lubrication theory, from asymptotic analysis, and from the complete Navier–Stokes solutions. Both quantities are overestimated by the lubrication model, although the flow rate not as much.

The results show that the meniscus location is one of the features most sensitive to parameter values and assumptions used in modelling the flow. Thus the agreement shown in figure 14 between experiments and Navier–Stokes theory, as calculated by the Galerkin/finite-element method, strongly confirms the latter. The flow rate λ has been found by Schneider (1962), Greener & Middleman (1979), and Benkreira *et al.* (1981) always to be approximately 1.3, with which the theory is also in accord.

Figure 15 displays another important prediction of the theory, the film-split ratio t_2/t_1, and compares it with experiments of Benkreira *et al.* (1981*b*). The slope of the asymptotic predictions (0.65) matches that of the data, but the measured values of

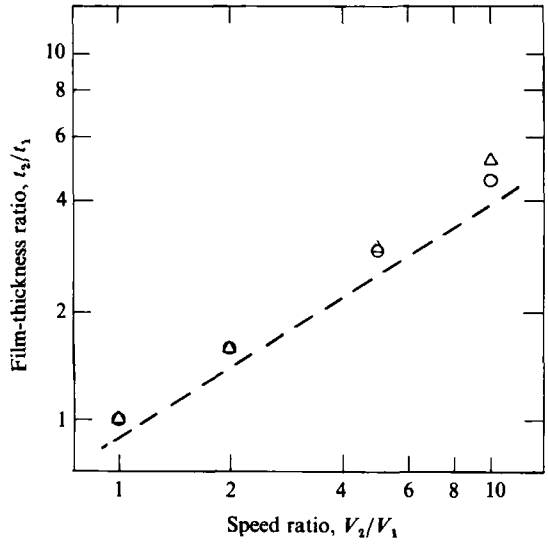

FIGURE 15. Comparison between theoretical prediction and experimental measurement of the film-thickness ratio. ○, asymptotic analysis; △, Navier–Stokes solutions; $Ca = \infty$, $Re = 0$, $St = 0$, $R/H_0 = 200$; ———, data of Benkreira *et al.* (1981).

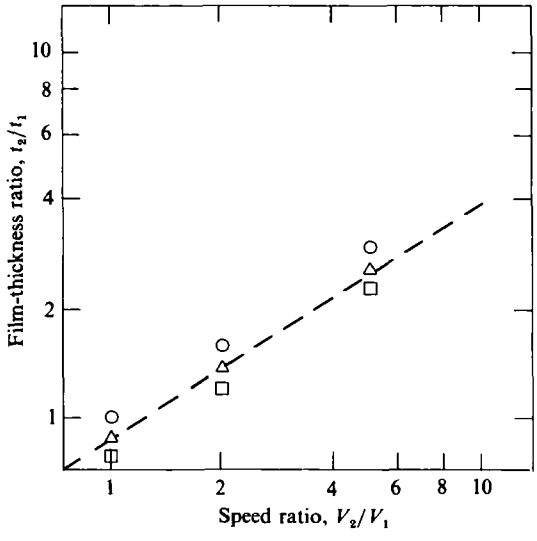

FIGURE 16. Calculations film-thickness ratio as a function of Stokes number. $St \equiv \rho g H_0^2/\mu \overline{V}$, $Ca = \infty$, $Re = 0$, $R/H_0 = 200$; ○, $St = 0$; △, $St = 0.1$; □, $St = 0.2$; ———; data of Benkreira *et al.* (1981).

t_2/t_1 are lower than predicted. Savage (1982) also reported data, but they differ from the others and scatter rather considerably (see his figure 4).

Benkreira *et al.* suggested that it is the action of gravity which causes their data to show an asymmetric split even though their speeds and roll radii were symmetric: they used one roll above the other; thus gravity acted across the gap and film 1 would be expected to be thicker. Finite-element calculations that account for gravity (figure 16) show that their explanation is likely, but more experiments are needed to clarify

this point, particularly experiments with gravity acting in a neutral direction (rolls side-by-side) and with mean film thickness measured accurately.

Perhaps the most significant aspect of these results is that they show exactly how and why the lubrication model breaks down. As already mentioned, the first stagnation line is not on the free surface but the onset of recirculating flow. Even if the pressure were constant across the recirculation to the free surface as postulated by Savage (1982), the lubrication model gives no clue as to where the free surface is located; thus its curvature cannot be estimated and surface-tension effects cannot be properly accounted for.

But an even more significant point is that the lubrication model never accurately predicts the asymmetric film split. The finite-element analysis proves that it is the local flow near the meniscus which determines the film split, *not* the upstream lubrication flow. The streamline passing through the first stagnation line downstream of the gap is *not* the one that divides the flow between the two rolls.

6. The special case of a roll and a stationary flat plate

This configuration has been investigated by Sullivan & Middleman (1979) and Baumann (1980). It is covered by the foregoing analyses when $R_1 \to \infty$ and $V_1 = 0$, so that the mean roll radius is $2R_2$ and the speed ratio V is infinite. For $V \to \infty$ the lubrication model predicts in the limit of infinite capillary number

$$\lambda = 1.25, \quad \tan\theta_m = 0.94. \tag{6.1}$$

The finite-element calculations corresponding to the asymptotic analysis of the flow near the meniscus were difficult at speed ratios exceeding 10 because of trouble in distributing appropriately the quadrilateral elements when the flow becomes highly asymmetric. It proved easier to carry out the full flow analysis described in §5 by starting from the symmetric case and merely changing the symmetry boundary condition to the no-slip condition on the same plane. In this limit of infinite speed ratio there is no splitting of the film between solid surfaces; rather the free-surface stagnation line which defines the split point becomes attached to the stationary solid surface. This introduces a new parameter: the static contact angle between the liquid and the stationary solid wall.

Figure 17 reveals that the flow rate through the gap is insensitive to the static contact angle that was chosen (in the range 60° to 140°), and that in the limit of infinite capillary number the flow rate is

$$\lambda = 1.23. \tag{6.2}$$

The lubrication model (6.1) agrees fairly well with this value. The film-split location ($\tan\theta_m$) is defined as the contact-line position, and is very sensitive to the specified static contact angle, as shown in figure 17. But the free-surface profiles in figure 18 make clear that the choice of contact angle affects only the flow near the contact line. These features agree with the results of the asymptotic analysis in §4. Moreover, according to the experiments of Sullivan & Middleman (1979) the flow rate falls in the range

$$1.1 \leqslant \lambda \leqslant 1.3, \tag{6.3}$$

with which the theoretical predictions agree.

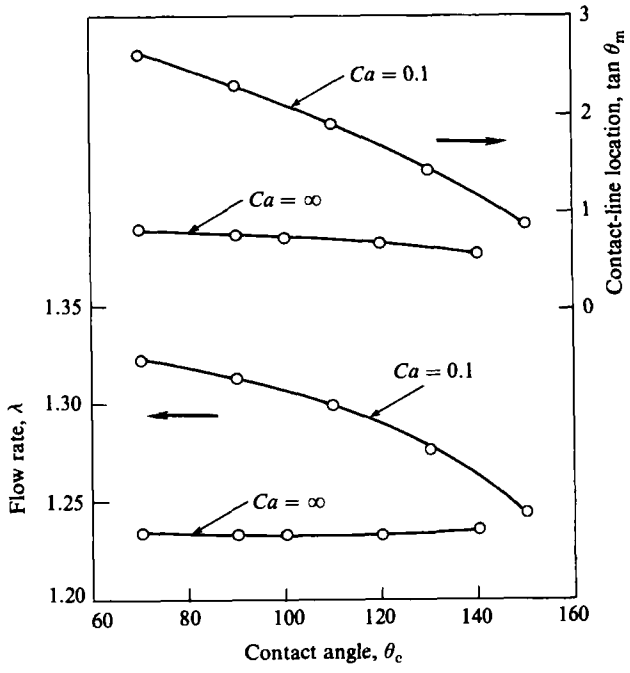

FIGURE 17. Sensitivity of flow rate (λ) and contact-line location ($\tan\theta_m$) to the specified static contact angle (θ_c) in the flow between a rotating roll and a stationary wall. $Re = 0$, $St = 0$, $R/H_0 = 2000$.

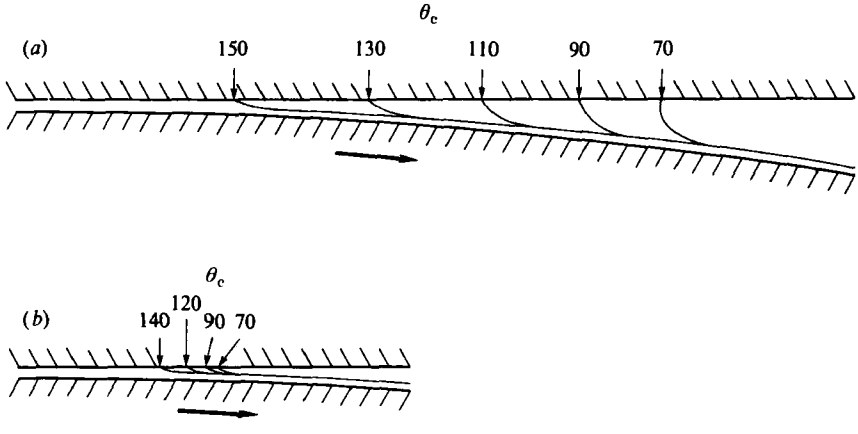

FIGURE 18. Sensitivity of free-surface profiles to specified static contact angle (θ_c) in the flow between a rotating roll and a stationary wall. $R/H_0 = 2000$, (*a*) $Ca = 0.1$, (*b*) $Ca = \infty$.

7. Concluding remarks

A general theory of steady, two-dimensional, Newtonian film-splitting flows in forward roll coating has been presented. The results show lubrication theory to be inadequate in predicting flow rate and film-split location for capillary numbers less than unity due to *ad hoc* boundary conditions that need be applied at the free surface. It is a useful approximation at high capillary numbers since overall flow rate is governed by lubrication flow when surface tension is negligible. One interesting

prediction of the lubrication model is that the ratio of film thicknesses produced on the rolls is equal to the 0.5 power of the speed ratio, and is independent of the roll radii and capillary number. The rigorous theory shows that the exponent should be approximately 0.65, and that for capillary numbers less than 0.1 the asymmetry of the film split is magnified. This speed-ratio dependence of the film-split ratio is confirmed by the data of Benkreira *et al.* (1981*b*), if the effect of gravity on their experiments is taken into account.

Comparison of the predictions of the most rigorous theory with those arising from the asymptotic expansions show the latter become accurate as H_0/R approaches 0.001 and remains accurate at lower values. The full solutions of the Navier–Stokes equations also give the full details of the two-dimensional flow field with its complex recirculation patterns in the asymmetric flow, and show how, in the limit of infinite speed ratio, the film-split stagnation line on the free surface evolves into a static contact line.

Both the asymptotic and full solutions to the Navier–Stokes equations governing film-splitting flows point out the inability of lubrication theory to accurately account for surface tension or to predict the asymmetric split. This proves that it is the local flow near the meniscus which governs the film split, not the upstream lubrication flow. Furthermore, this local two-dimensional flow will be even more important in determining the stability of film-splitting flows to 'ribbing'. The full solutions set the stage for accurate three-dimensional stability analysis (Coyle 1984; Coyle *et al.* 1986*a*).

The authors wish to thank S. F. Kistler, H. Saito, N. E. Bixler, and K. J. Ruschak for many helpful discussions. This work was supported by 3M Company and the University of Minnesota Computer Center.

REFERENCES

Banks, W. H. & Mill, C. C. 1954 Some observations on the behaviour of liquids between rotating rollers. *Proc. R. Soc. Lond.* A **223**, 414.

Baumann, T. M. 1980 Roll coating in the presence of a stationary constraint. M.S. thesis, University of Massachusetts.

Benkreira, H., Edwards, M. F. & Wilkinson, W. L. 1981*a* A semi-empirical model of the forward roll coating flow of Newtonian fluids. *Chem. Engng Sci.* **36**, 423.

Benkreira, H., Edwards, M. F. & Wilkinson, W. L. 1981*b* Roll coating of purely viscous liquids. *Chem. Engng Sci.* **36**, 429.

Benkreira, H., Edwards, M. F. & Wilkinson, W. L. 1982 Flux distribution in forward roll coating: a simple analysis. *Chem. Engng J.* **25**, 211.

Bixler, N. E. 1982 Stability of a coating flow. Ph.D. thesis, University of Minnesota.

Cameron, A. 1966 *Basic Lubrication Theory.* Wiley.

Cole, J. A. & Hughes, C. J. 1956 Oil flow and film extent in complete journal bearings. *IME Proceedings* **170** (17), 499.

Coyle, D. J. 1984 The fluid mechanics of roll coating: steady flows, stability, and rheology. Ph.D. thesis, University of Minnesota.

Coyle, D. J., Macosko, C. W. & Scriven, L. E. 1982 Computer simulation of nip flow in roll coating. In *Computer Applications in Applied Polymer Science* (ed. T. Provder), p. 251. ACS Symposium Series 197, American Chemical Society, Washington.

Coyle, D. J., Macosko, C. W. & Scriven, L. E. 1986*a* Stability of symmetric film-splitting between counterrotating cylinders. *J. Fluid Mech.* (submitted).

COYLE, D. J., MACOSKO, C. W. & SCRIVEN, L. E. 1986*b* Film-splitting flows in forward roll coating of shear-thinning liquids. *AIChE J.* (submitted).

COYNE, J. C. & ELROD, H. G. 1970 Conditions for the rupture of a lubricating film. Part I: Theoretical model; Part II: New boundary conditions for Reynolds equations. *Trans. ASME* F: *J. Lubric. Tech.* **92**, 451.

DOWSON, D. & TAYLOR, C. M. 1979 Cavitation in bearings. *Ann. Rev. Fluid Mech.* **11**, 35.

FLOBERG, L. 1961*a* Lubrication of two cylindrical surfaces considering cavitation. *Trans. Chalmers Univ. Technol.* 234, Goteborg.

FLOBERG, L. 1961*b* On hydrodynamic lubrication with special reference to cavitation in bearings. Dissertation, Chalmers Univ. Technol. 30, Goteborg.

FLOBERG, L. 1964 Cavitation in lubricating oil films. In: *Cavitation in Real Liquids* (ed. R. Davies). Elsevier.

GARTLING, D. K., NICKELL, R. E. & TANNER, R. I. 1977 A finite element convergence study for accelerating flow problems. *Intl J. Numer. Meth. Engng* **11**, 1155.

GATCOMBE, E. K. 1945 Lubrication characteristics of involute spur gears – a theoretical investigation. *Trans. ASME* **67**, 177.

GREENER, J. 1979 Bounded coating flows of viscous and viscoelastic fluids. Ph.D. thesis, University of Massachusetts.

GREENER, J. & MIDDLEMAN, S. 1975 A theory of roll coating of viscous and viscoelastic fluids. *Polymer Engng Sci.* **15**, 1.

GREENER, J. & MIDDLEMAN, S. 1979 Theoretical and experimental studies of the fluid dynamics of a two-roll coater. *I & EC Fund.* **18**, 35.

HINTERMAIER, J. C. & WHITE, R. E. 1965 The splitting of a water film between rotating rolls. *Tappi* **48**, 617.

HOFFMAN, R. D. & MYERS, R. R. 1962 The splitting of thin liquid films. Cavitation dynamics. *Trans. Soc. Rheol.* **6**, 197.

HOOD, P. 1976 Frontal solution program for unsymmetric matrices. *Intl J. Numer. Meth. Engng* **10**, 379.

HOOD, P. 1977 Correction. *Intl J. Numer. Meth. Engng* **11**, 1055.

HOPKINS, M. R. 1957 Viscous flow between rotating cylinders and a sheet moving between them. *Br. J. Appl. Phys.* **8**, 443.

KISTLER, S. F. 1983 The fluid mechanics of curtain coating and related viscous free surface flows. Ph.D. thesis, University of Minnesota.

KISTLER, S. F. & SCRIVEN, L. E. 1983 Coating flows. In: *Computational Analysis of Polymer Processing* (ed. J. R. A. Pearson & S. M. Richardson), p. 243. London and New York: Applied Science.

KISTLER, S. F. & SCRIVEN, L. E. 1984 Coating flow theory by finite element and asymptotic analysis of the Navier–Stokes system. *Intl J. Numer. Meth. Fluids* **4**, 207.

MIDDLEMAN, S. 1977 *Fundamentals of Polymer Processing*. McGraw-Hill.

MILLER, J. C. & MYERS, R. R. 1958 A photographic study of liquid flow in a roll nip. *Trans. Soc. Rheol.* **2**, 77.

MYERS, R. R. & HOFFMAN, R. D. 1961 The distribution of pressures in the roll application of Newtonian fluids. *Trans. Soc. Rheol.* **5**, 317.

MYERS, R. R., MILLER, J. C. & ZETTLEMOYER, A. C. 1959 The splitting of thin liquid films: kinematics. *J. Colloid Sci.* **14**, 287.

NICKELL, R. E., TANNER, R. I. & CASWELL, B. 1974 Solution of viscous incompressible jet and free surface flows using finite element methods. *J. Fluid Mech.* **65**, 189.

PITTS, E. & GREILLER, J. 1961 The flow of thin liquid films between rollers. *J. Fluid Mech.* **11**, 33.

REYNOLDS, O. 1886 On the theory of lubrication and its application to Mr Beauchamp Tower's experiments including an experimental determination of the viscosity of olive oil. *Phil. Trans. R. Soc. Lond.* A **177**, 157.

RUSCHAK, K. J. 1980 A method for incorporating free boundaries with surface tension in finite element fluid flow simulators. *Intl J. Numer. Meth. Engng* **15**, 639.

RUSCHAK, K. J. 1982 Boundary conditions at a liquid/air interface in lubrication flows. *J. Fluid Mech.* **119**, 107.

SAITO, H. & SCRIVEN, L. E. 1981 Study of coating flow by the finite element method. *J. Comp. Phys.* **42**, 53.

SAVAGE, M. D. 1977 Cavitation in lubrication. Part 1: On boundary conditions and cavity–fluid interfaces. Part 2: Analysis of wavy interfaces. *J. Fluid Mech.* **80**, 743.

SAVAGE, M. D. 1982 Mathematical models for coating processes. *J. Fluid Mech.* **117**, 443.

SCHNEIDER, G. B. 1962 Analysis of forces causing flow in roll coaters. *Trans. Soc. Rheol.* **6**, 209.

SILLIMAN, W. J. 1979 Viscous film flows with contact lines. Ph.D. thesis, University of Minnesota, Minneapolis.

SILLIMAN, W. J. & SCRIVEN, L. E. 1980 Separating flow near a static contact line: slip at a wall and shape of a free surface. *J. Comp. Phys.* **34**, 287.

SULLIVAN, T. M. & MIDDLEMAN, S. 1979 Roll coating in the presence of a fixed constraining boundary. *Chem. Engng Commun.* **3**(6), 469.

TAYLOR, C. M. 1974 Film rupture for a lubricated cylinder lightly loaded against a plane. *J. Mech. Engng Sci.* **16**, 225.

TAYLOR, G. I. 1963 Cavitation of a viscous fluid in narrow passages. *J. Fluid Mech.* **16**, 595.

VAN DYKE, M. 1975 *Perturbation Methods in Fluid Mechanics.* Stanford, CA: Parabolic.

WALTERS, R. A. 1980 The frontal method in hydrodynamics simulations. *Comp. Fluids* **8**, 265.

WILLIAMSON, A. S. 1972 The tearing of an adhesive layer between flexible tapes pulled apart. *J. Fluid Mech.* **52**, 639.